MS.ID-IJPBS-2866
International Journal of Pharmacy and Biological Sciences-IJPBS™ (2025) 15 (2): 164-175
Online ISSN: 2230-7605, Print ISSN: 2321-3272
Research Article | Pharmaceutical Sciences | OA Journal | MCI Approved | Index Copernicus

Novel Amide Functionalized Pyrimidine Derivative as Potential Anticancer Agents: Synthesis, Characterization, Molecular Docking and *Invitro* Cytotoxicity Evaluation

K. Jyothi*[1] and M. Kannadasan[2]

[1*]**Research Scholar, Faculty of Pharmaceutical Sciences, Motherhood University, Dehradun Road, Village Karoundi Post - Bhagwanpur, Roorkee Tehsil, Haridwar Distt., Uttarakhand 247661.**

[2]**Professor and Principal, Faculty of Pharmaceutical Sciences, Motherhood University, Dehradun Road, Village Karoundi Post - Bhagwanpur, Roorkee Tehsil, Haridwar Distt., Uttarakhand 247661.**

Received: 20 Jan 2025 / Accepted: 24 Mar 2025/ Published online: 01 April 2025
***Corresponding Author Email:** jyothikasapogu214@gmail.com

Abstract

A series of amide-functionalized pyrimidine derivatives (**6a–6r**) were synthesized via a three-step route involving (1) multicomponent assembly of 2-(4-methylpyrimidin-5-yl) acetonitrile (**4**), (2) $LiAlH_4$ reduction to the primary amine (**5**), and (3) DCC/DMAP-mediated coupling with diverse carboxylic acids. The compounds were obtained in good yields (65–92%) and high purity (>95%, NMR/HRMS). Molecular docking studies against EGFR (PDB: 6LUD) and CDK-4 (PDB: 7SJ3) revealed strong binding affinities for hydroxy-substituted derivatives, particularly **6k** (EGFR: −7.245 kcal/mol), **6j** (CDK-4: −8.72 kcal/mol), and **6l** (CDK-4: −9.23 kcal/mol), highlighting the role of hydrogen-bonding interactions. Cytotoxicity screening (MTT assay) against A-549 (lung), HCT-116 (colorectal), PANC-1 (pancreatic), and HaLa (cervical) cancer cells identified **6l** (2-hydroxy-4-methoxyphenyl) as the most potent inhibitor (IC_{50} = 5.87–7.86 µM), with 3–7-fold selectivity over normal HEK-293 cells. Structure-activity relationships demonstrated that electron-donating hydroxy/methoxy groups enhanced activity, while nitro or bulky substituents reduced potency. Notably, **6j** (3,4-dihydroxyphenyl) exhibited exceptional activity against HCT-116 (IC_{50} = 5.67 µM), correlating with its high CDK-4 binding affinity. The combined in silico and in vitro results suggest that these pyrimidine hybrids act via dual EGFR/CDK-4 inhibition, with **6b**, **6j**, and **6l** emerging as promising anticancer leads due to their potent cytotoxicity, kinase selectivity, and favorable safety profiles. This study provides a robust framework for further optimization of pyrimidine-based therapeutics.

Keywords

Pyrimidine derivatives, Multicomponent synthesis, EGFR, CDK-4, Molecular docking, Anticancer activity.

*****

INTRODUCTION

Cancer remains a formidable global health challenge. In 2023 alone, an estimated 20.01 million new cases were diagnosed worldwide and 9.6 million individuals succumbed to the disease [1]. Although the past few decades have witnessed formidable progress—including advances in surgery, precision radiotherapy, immuno-oncology, and image-guided interventions—cancer continues to exact a substantial toll on population health [2,3]. Among the standard treatment modalities, systemic chemotherapy still occupies a pivotal position because of its broad spectrum of activity and its clinical synergy with surgery and radiation [4,5]. Nevertheless, conventional chemotherapeutic agents often lack tumour selectivity, producing significant acute toxicities (myelosuppression, mucositis, cardiotoxicity) and late-stage sequelae (secondary malignancies, organ dysfunction) that are distressing to patients and complicate long-term disease management [6]. The pressing need for safer and more efficacious therapeutics therefore drives an intense search for molecularly targeted anticancer drugs that can discriminate between malignant and normal tissues.

The quest for selectivity faces two formidable hurdles: first, the close genetic and metabolic resemblance of normal and transformed cells; second, the inherent heterogeneity of tumours, which vary not only between patients but also within individual lesions [7]. These factors underscore the importance of designing agents that exploit discrete oncogenic dependencies—often specific signalling nodes or cell-cycle checkpoints—while sparing healthy cells.

Within this context, nitrogen-containing heterocycles, and pyrimidines in particular, have emerged as privileged scaffolds in modern oncology. Several clinically approved tyrosine-kinase inhibitors—Pazopanib, Nilotinib, Imatinib, and Dasatinib—share a pyrimidine core (**Figure 1**) as their pharmacophoric anchor [8]. These drugs exert potent antitumor activity by occupying the adenine pocket of protein kinases and disrupting signal transduction pathways critical for tumor growth. A prominent example is the epidermal growth factor receptor tyrosine kinase (EGFR-TK); pyrimidine-based inhibitors arrest its ATP-dependent autophosphorylation, thereby quenching downstream proliferative and anti-apoptotic signalling [9,10]. Because aberrant EGFR expression or mutation drives a spectrum of malignancies—including non-small-cell lung, colorectal, and glioblastoma—EGFR-TK has become one of the most exhaustively characterized and clinically validated cancer targets [11,12]. Constitutive activation of EGFR or other receptor tyrosine kinases promotes uncontrolled cell division, invasion, metastasis, and resistance to therapy, underpinning their central role in oncogenesis [13].

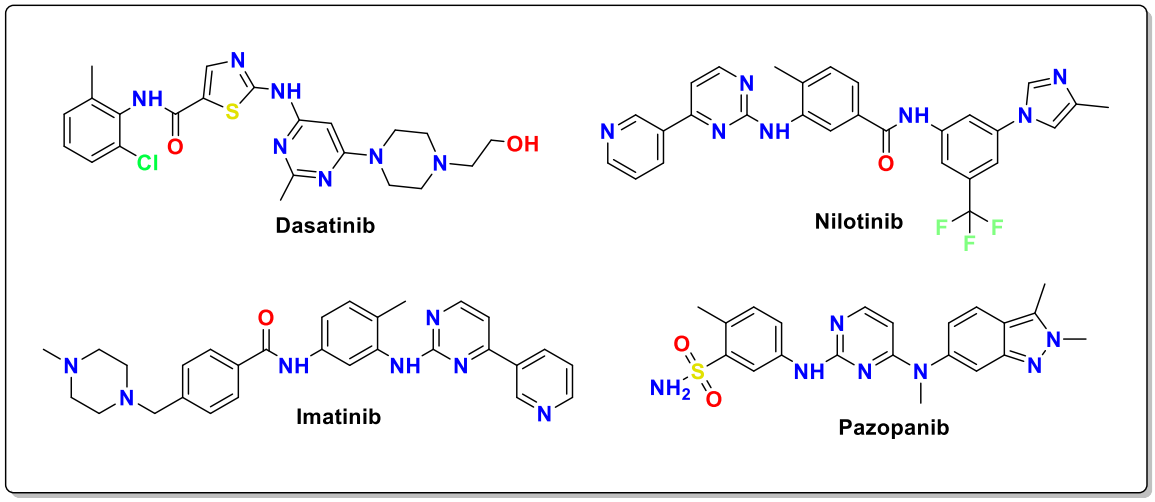

Figure 1: Marketed anticancer drugs with pyrimidine scaffold

Pyrimidine scaffolds also lend themselves to inhibition of cyclin-dependent kinase 4 (CDK-4), a master regulator of G1-phase progression. CDK-4 forms a complex with cyclin D to phosphorylate the retinoblastoma protein, thereby relieving its suppression of E2F transcription factors and driving entry into S-phase. Pharmacological blockade of CDK-4 induces cell-cycle arrest and has shown substantial clinical benefit, exemplified by the success of CDK-4/6 inhibitors in hormone-receptor-positive breast cancer [14]. Thus, EGFR-TK and CDK-4 together constitute compelling, mechanistically distinct targets for the development of next-generation anticancer agents.

Guided by these considerations, we have designed a series of amide-functionalized pyrimidine hybrids that merge the kinase-affinity profile of the pyrimidine nucleus with an amide linker capable of hydrogen bonding and conformational restraint. The new derivatives were synthesized and assessed for in-vitro cytotoxicity against four human cancer cell lines, alongside a normal human cell line to gauge selectivity. Complementary molecular-docking studies against EGFR (PDB 6LUD) and CDK-4 (PDB 7SJ3) were undertaken to elucidate binding modes and rationalize observed activity profiles. This integrated approach aims to identify candidates with an improved therapeutic index, addressing the dual imperatives of potency and safety that define contemporary anticancer drug discovery.

MATERIALS AND METHODS

All reagents and solvents utilized in the study were of synthetic grade and procured from Sigma-Aldrich, Bangalore, India, and used as received without further purification. Reaction progress was monitored by thin-layer chromatography (TLC) on Merck-precoated aluminum plates containing silica gel 60 F_{254}. Visualization of spots was carried out using iodine vapors and under UV light. Melting points of the synthesized compounds were determined using a Remi electronic melting point apparatus.

The structural characterization of the synthesized compounds was performed using nuclear magnetic resonance (NMR) spectroscopy. ^{1}H and ^{13}C NMR spectra were recorded on a BRUKER DRX instrument. Chemical shift values (δ) were reported in parts per million (ppm) relative to the internal standard tetramethyl silane (TMS). The multiplicities of the signals were denoted as singlet (s), doublet (d), triplet (t), quartet (q), and multiplet (m). High-resolution mass spectra (HRMS) were obtained using a Waters Xevo Q-Tof mass spectrometer to confirm the molecular weights of the synthesized compounds.

Synthesis of Amide Functionalized Pyrimidine Derivatives

Multicomponent synthesis of di-substituted pyrimidine (2-(4-methylpyrimidin-5-yl) acetonitrile) (4)

The reaction conducted by mixing the substituted enamine (1 equiv**,** 10mmol) with ortho ester (3 equiv, 30mmol) and ammonium acetate (3 equiv, 20mmol) in benzene or toluene at 70-80C under reflux conditions using the Lewis acid zinc chloride or aluminium chloride as catalyst [15-18].

The reaction was continuously monitored by TLC under UV- Light. After completion of reaction basic work up procedure with sodium bicarbonate was applied to get the crude product of pyrimidine. The intermediate product was isolated from the column chromatography by ethyl acetate: hexane (1:9 v/v) mobile phase system and purified by recrystallization in ethanol.

Procedure for the synthesis of 2-(4-methylpyrimidin-5-yl) ethan-1-amine (5) intermediate

The reduction of 2-(4-methylpyrimidin-5-yl) acetonitrile to the corresponding primary amine was performed under inert atmosphere. A flame-dried 25 mL round-bottom flask equipped with a magnetic stirrer was charged with 2-(4-methylpyrimidin-5-yl) acetonitrile (1.0 mmol) dissolved in anhydrous THF (10 mL). The solution was cooled to 0 °C in an ice bath, and lithium aluminum hydride ($LiAlH_4$, 3.0 equiv, 114 mg) was added portion wise over 10 min to control exothermicity. After complete addition, the reaction was warmed to room temperature and stirred for 3 h (monitored by TLC, CH_2Cl_2/MeOH 9:1). The reaction was carefully quenched at 0 °C by sequential dropwise addition of H_2O (0.1 mL), 15% NaOH (aq, 0.1 mL), and additional H_2O (0.3 mL), followed by stirring for 15 min. The mixture was filtered through a Celite pad, washed with THF (3 × 5 mL), and concentrated under reduced pressure. The crude product was purified by flash chromatography (SiO_2, CH_2Cl_2/MeOH/NH_4OH 90:9:1) to afford 2-(4-methylpyrimidin-5-yl) ethan-1-amine as a solid [19, 20].

General Procedure for the synthesis of Amide Functionalized Pyrimidine Derivatives (6a-6r)

The carboxylic acid **(a-r)** (1.0 mmol, 1.0 equiv) was dissolved in dry dichloromethane (DCM) (10 mL per 1 mmol of carboxylic acid) in a reaction flask equipped with a magnetic stir bar. To this solution, N, N'-dicyclohexyl carbodiimide (DCC) (1.2 equiv) was added while stirring in an ice bath, and the mixture was stirred for 15-30 minutes. Subsequently, 4-dimethylaminopyridine (DMAP) (0.1 equiv) was added to the reaction mixture. The primary amine **5** (1.0 equiv) was then added slowly while maintaining stirring in the ice bath. The reaction mixture was allowed to gradually warm to room temperature and stirred for 18 hours, with the progress monitored by thin-layer chromatography (TLC). Upon completion, the reaction was quenched by adding water (10 mL), and the mixture was extracted with DCM (3 x 20 mL). The combined organic layers were washed with saturated sodium bicarbonate solution (2 x 20 mL) and brine (20 mL), then dried over anhydrous magnesium sulfate (MgSO4). After filtration through Whatman filter paper, the solvent was removed under reduced pressure using a rotary evaporator. The crude product was purified by column

chromatography on silica gel using hexane:ethyl acetate (8:2 v/v) as the eluent [21].

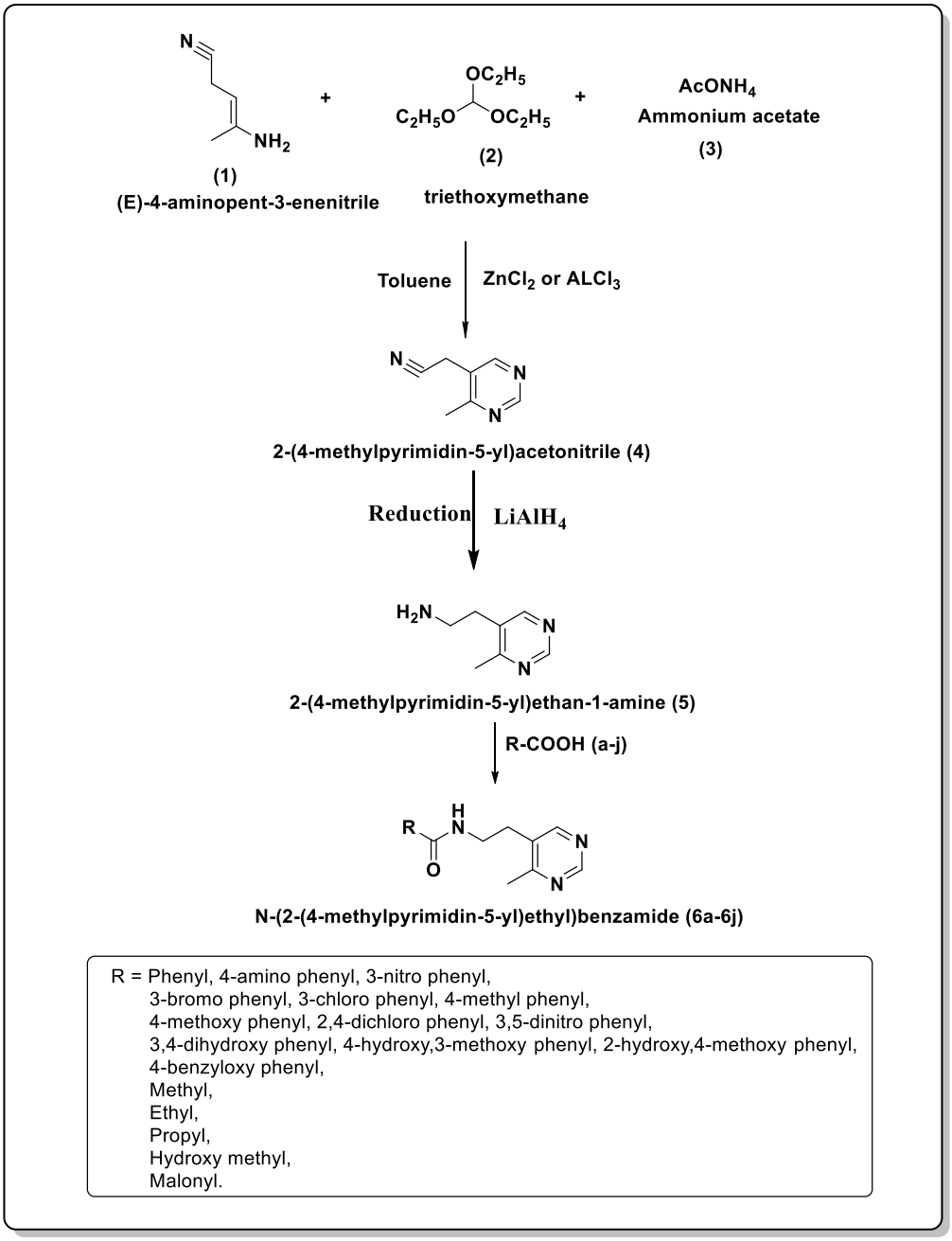

Figure 2: Scheme of Synthesis for the amide functionalized pyrimidine derivatives 6a-6r

Molecular Docking

The X-ray crystal structures of EGFR (6LUD) and two CDK-4 (7SJ3) domains were obtained from the Protein Data Bank. The Protein Preparation Wizard module of Schrödinger software was used to prepare the protein complex by introducing hydrogen atoms and allocating bond orders to the protein's 3D structure. The LigPrep module of Schrödinger software was used to prepare ligands with defined chirality and optimize their 3D structures using the OPLS 2005 force field. The receptor sites for 6LUD and 7SJ3 were analysed using the SITEMAP ANALYSIS TOOL of Maestro 11.8, and receptor grids were generated using the grid generation tool of Schrödinger suite. Molecular docking was performed using the Glide program's extra-precision docking modes (Glide XP), and the XP Glide score was calculated using the binding interaction energy, van der Waals energy, electrostatic potential energy, and strain energy. The binding interaction of the ligands to the active site of EGFR and CDK-4 was examined using Schrödinger Maestro interface [22].

MTT assay

The cytotoxicity and cell viability of amide functionalized pyrimidine derivatives (6a-6r) were assessed using the MTT (3-(4,5-dimethylthiazol-2-yl)-2,5-diphenyltetrazolium bromide) assay. Several human cancer cell lines, such as A-549 (Non-Small Cell Lung Cancer), HCT-116 (Colorectal Cancer), PANC-1 (Pancreatic cancer), and HaLa (Cervical cancer), along with one normal Human Embryonic Kidney Cell line (HEK-293), were cultured in 96-well plates and given time to adhere overnight. Subsequently, the cells were subjected to different concentrations (0.1 µM, 10 µM, 50 µM, and 100 µM) of the synthesised 1H-1,2,4-triazole-3-carboxamide derivatives 4a-4n for incubation periods of 24, 48, or 72 hours. After the designated incubation period, MTT solution was introduced into each well, and the plates were subsequently incubated to facilitate the formation of formazan crystals. The formazan crystals were solubilized in dimethyl sulfoxide (DMSO), and the absorbance was quantified using a microplate reader. The relationship between absorbance values and cell viability was analyzed, where lower absorbance values correlated with increased cytotoxicity and reduced cell viability. Data obtained from the MTT assay across different concentrations and time points were scrutinized to determine the half-maximal inhibitory concentration (IC50) values of the amide functionalized pyrimidine derivatives (6a-6r) for each cell line. The experiments were replicated three times, including suitable controls to validate the precision and consistency of the assay results [23].

RESULTS AND DISCUSSION

Chemistry

A three-step synthesis afforded target compounds in good yields (65–92%). First, a multicomponent reaction of enamine, ortho ester, and NH_4OAc with $ZnCl_2/AlCl_3$ catalysis yielded 2-(4-methylpyrimidin-5-yl) acetonitrile (4, 78%). $LiAlH_4$ reduction of 4 gave the primary amine 5 (85%), which was coupled with diverse carboxylic acids (a–r) via DCC/DMAP activation. Purification by column chromatography provided final products 6a-6r, confirmed by NMR and HRMS (>95% purity). The efficient route enables broad structural diversification for biological studies. Following section enumerates the spectral characterization of the compounds.

Analytical Characterization of synthesized derivatives

6a: N-(2-(4-methylpyrimidin-5-yl) ethyl) benzamide

^{1}H NMR (500 MHz, DMSO-d_6) δ 8.73 (d, *J* = 1.7 Hz, 1H), 8.66 (t, *J* = 4.9 Hz, 1H), 8.40 (d, *J* = 1.6 Hz, 1H), 7.81 (dd, *J* = 8.2, 1.3 Hz, 2H), 7.58 – 7.50 (m, 1H), 7.43 (t, *J* = 8.0 Hz, 2H), 3.51 (td, *J* = 6.0, 4.9 Hz, 2H), 2.91 (t, *J* = 6.1 Hz, 2H), 2.29 (s, 3H). **^{13}C NMR (120 MHz, Chloroform-*d*) δ** 166.98, 159.35, 156.16, 153.29, 134.47, 132.47, 131.89, 128.38, 127.17, 40.38, 29.23, 21.82. **HRMS:** m/z: For $C_{14}H_{15}N_3O$ ([M + H]+): 242.1209, found 242.01205.

6b: 2-hydroxy-N-(2-(4-methylpyrimidin-5-yl) ethyl) benzamide

^{1}H NMR (500 MHz, DMSO-d_6) δ 11.80 (s, 1H), 8.66 (d, *J* = 1.9 Hz, 1H), 8.32 (d, *J* = 1.6 Hz, 1H), 8.11 (t, *J* = 4.9 Hz, 1H), 7.70 (dd, *J* = 7.9, 1.6 Hz, 1H), 7.39 (td, *J* = 8.0, 1.5 Hz, 1H), 7.30 (td, *J* = 7.9, 1.5 Hz, 1H), 7.04 (dd, *J* = 8.4, 1.5 Hz, 1H), 3.55 (td, *J* = 6.0, 4.9 Hz, 2H), 2.95 (t, *J* = 6.1 Hz, 2H), 2.28 (s, 3H). **^{13}C NMR (120 MHz, Chloroform-*d*) δ** 170.68, 160.60, 159.92, 156.16, 153.29, 133.97, 132.52, 128.77, 119.01, 117.51, 116.03, 41.06, 29.75, 22.36. **HRMS:** m/z: For $C_{14}H_{15}N_3O_2$ ([M + H] +): 257.1217, found 257.1214.

6c: N-(2-(4-methylpyrimidin-5-yl) ethyl)-3-nitrobenzamide

^{1}H NMR (500 MHz, DMSO-d_6) δ 8.79 (d, *J* = 1.7 Hz, 1H), 8.71 (t, *J* = 5.0 Hz, 1H), 8.65 (t, *J* = 2.2 Hz, 1H), 8.46 – 8.38 (m, 2H), 8.13 – 8.06 (m, 1H), 7.73 (t, *J* = 8.5 Hz, 1H), 3.45 (q, *J* = 5.8 Hz, 2H), 2.86 (t, *J* = 6.1 Hz, 2H), 2.29 (s, 3H). **^{13}C NMR (120 MHz, Chloroform-*d*) δ** 166.34, 159.15, 156.16, 153.29, 147.85, 135.49, 133.21, 132.47, 130.28, 125.83, 122.13, 39.54, 29.97, 21.34. **HRMS:** m/z: For $C_{14}H_{14}N_4O_3$ ([M + H]+): 287.1186, found 287.1185.

6d: 3-bromo-N-(2-(4-methylpyrimidin-5-yl) ethyl) benzamide

^{1}H NMR (500 MHz, DMSO-d_6) δ 8.71 (d, *J* = 1.7 Hz, 1H), 8.51 (t, *J* = 5.0 Hz, 1H), 8.35 (d, *J* = 1.6 Hz, 1H), 7.96 (t, *J* = 2.2 Hz, 1H), 7.81 (ddd, *J* = 8.3, 2.2, 1.1 Hz, 1H), 7.73 – 7.67 (m, 1H), 7.37 (t, *J* = 8.1 Hz, 1H), 3.45 (td, *J* = 6.0, 4.9 Hz, 2H), 2.88 (t, *J* = 6.1 Hz, 2H), 2.28 (s, 3H). **^{13}C NMR (120 MHz, Chloroform-*d*) δ** 166.04, 159.35, 156.16, 153.29, 134.53, 133.72, 132.47, 131.03, 130.59, 126.52, 120.72, 40.77, 30.19, 22.36. **HRMS:** m/z: For $C_{14}H_{14}BrN_3O$ ([M + H]+): 321.0327, found 321.0323.

6e: 3-chloro-N-(2-(4-methylpyrimidin-5-yl) ethyl) benzamide

^{1}H NMR (500 MHz, DMSO-d_6) δ 8.73 (d, *J* = 1.7 Hz, 1H), 8.51 (t, *J* = 5.0 Hz, 1H), 8.31 (d, *J* = 1.6 Hz, 1H), 7.91 (t, *J* = 2.2 Hz, 1H), 7.82 – 7.76 (m, 1H), 7.63 (dt, *J* = 8.1, 1.7 Hz, 1H), 7.51 (t, *J* = 8.0 Hz, 1H), 3.45 (td, *J* = 6.0, 4.9 Hz, 2H), 2.86 (t, *J* = 6.1 Hz, 2H), 2.26 (s, 3H). **^{13}C NMR (120 MHz, Chloroform-*d*) δ** 167.47, 159.35, 156.16, 153.29, 134.45, 133.75, 132.47, 130.58, 130.03, 127.79, 126.21, 40.77, 29.75, 22.07. **HRMS:** m/z: For $C_{14}H_{14}ClN_3O$ ([M + H] +): 277.0851, found 277.0849.

6f: 4-methyl-N-(2-(4-methylpyrimidin-5-yl) ethyl) benzamide

^{1}H NMR (500 MHz, DMSO-d_6) δ 8.73 (d, *J* = 1.7 Hz, 1H), 8.60 (t, *J* = 5.0 Hz, 1H), 8.35 (d, *J* = 1.5 Hz, 1H), 7.77 (d, *J* = 8.0 Hz, 2H), 7.29 (d, *J* = 8.0 Hz, 2H), 3.46 (q, *J* = 5.8 Hz, 2H), 2.90 (s, 2H), 2.31 (s, 3H), 2.25 (s, 3H). **^{13}C NMR (120 MHz, Chloroform-*d*) δ** 168.51, 160.37, 156.16, 153.29, 140.76, 132.47, 131.74, 128.93, 127.68, 40.04, 28.74, 22.36, 21.85. **HRMS:** m/z: For $C_{15}H_{17}N_3O$ ([M + H]+): 256.1395, found 256.1395.

6g: 4-methoxy-N-(2-(4-methylpyrimidin-5-yl) ethyl) benzamide

^{1}H NMR (500 MHz, DMSO-d_6) δ 8.73 (d, *J* = 1.7 Hz, 1H), 8.54 (t, *J* = 4.9 Hz, 1H), 8.35 (d, *J* = 1.6 Hz, 1H), 7.80 (d, *J* = 8.4 Hz, 2H), 6.98 (d, *J* = 8.3 Hz, 2H), 3.75 (s, 3H), 3.43 (td, *J* = 6.0, 4.8 Hz, 2H), 2.89 (t, *J* = 6.1 Hz, 2H), 2.29 (s, 3H). **^{13}C NMR (120 MHz, Chloroform-*d*) δ** 168.20, 162.38, 159.92, 156.16, 153.29, 132.47, 130.63, 126.98, 113.35, 54.54, 40.77, 29.46, 22.36. **HRMS:** m/z: For $C_{15}H_{17}N_3O_2$ ([M + H]+): 272.1416, found 272.1411.

6h: 2,4-dichloro-N-(2-(4-methylpyrimidin-5-yl)ethyl)benzamide

^{1}H NMR (500 MHz, DMSO-d_6) δ 8.73 (d, *J* = 1.7 Hz, 1H), 8.43 (t, *J* = 5.0 Hz, 1H), 8.36 (d, *J* = 1.6 Hz, 1H), 7.61 (d, *J* = 8.5 Hz, 1H), 7.49 (d, *J* = 2.1 Hz, 1H), 7.39 (dd, *J* = 8.4, 2.1 Hz, 1H), 3.49 (td, *J* = 6.0, 4.9 Hz, 2H), 2.89 (t, *J* = 6.1 Hz, 2H), 2.31 (s, 3H). **^{13}C NMR (120 MHz, Chloroform-*d*) δ** 166.96, 159.92, 156.16, 153.29, 136.70, 133.08, 132.49 (d, *J* = 3.5 Hz), 130.01, 129.34, 127.38, 40.77, 29.75, 22.57. **HRMS:** m/z: For $C_{14}H_{13}Cl_2N_3O$ ([M + H]+): 311.0423, found 311.0421.

6i: N-(2-(4-methylpyrimidin-5-yl)ethyl)-3,5-dinitrobenzamide

^{1}H NMR (500 MHz, DMSO-d_6) δ 8.96 (t, *J* = 2.2 Hz, 1H), 8.91 (d, *J* = 2.3 Hz, 2H), 8.82 (t, *J* = 5.0 Hz, 1H), 8.77 (d, *J* = 1.7 Hz, 1H), 8.35 (d, *J* = 1.6 Hz, 1H), 3.46 (td, *J* = 6.0, 4.9 Hz, 2H), 2.89 (t, *J* = 6.1 Hz, 2H), 2.31 (s, 3H). **^{13}C NMR (120 MHz, Chloroform-*d*) δ** 165.75, 159.92, 156.16, 153.29, 148.46, 136.57, 132.47, 127.61, 121.23, 39.83, 28.74, 22.07. **HRMS:** m/z: For $C_{14}H_{13}N_5O_5$ ([M + H]+): 332.2851, found 332.2847.

6j: 3, 4-dihydroxy-N-(2-(4-methylpyrimidin-5-yl) ethyl) benzamide

^{1}H NMR (500 MHz, DMSO-d_6) δ 8.71 (d, *J* = 1.7 Hz, 1H), 8.63 (t, *J* = 4.9 Hz, 1H), 8.45 (s, 1H), 8.40 (d, *J* = 1.6 Hz, 1H), 7.44 – 7.37 (m, 2H), 7.32 (d, *J* = 2.1 Hz, 1H), 6.87 (d, *J* = 9.1 Hz, 1H), 3.49 (td, *J* = 6.0, 4.9 Hz, 2H), 2.91 (t, *J* = 6.1 Hz, 2H), 2.29 (s, 3H). **^{13}C NMR (120 MHz, Chloroform-*d*) δ** 167.47, 159.92, 156.16, 153.29, 148.77, 146.31, 132.47, 126.04, 120.16, 116.15, 114.44, 40.77, 29.97, 22.36. **HRMS:** m/z: For $C_{14}H_{15}N_3O_3$ ([M + H]+): 274.1208, found 274.1206.

6k: 4-hydroxy-3-methoxy-N-(2-(4-methylpyrimidin-5-yl) ethyl)benzamide

^{1}H NMR (500 MHz, DMSO-d_6) δ 9.56 (s, 1H), 8.82 (d, *J* = 1.7 Hz, 1H), 8.62 (t, *J* = 5.1 Hz, 1H), 8.40 (d, *J* = 1.6 Hz, 1H), 7.52 (dd, *J* = 8.8, 1.9 Hz, 1H), 7.35 (d, *J* = 2.1 Hz, 1H), 6.91 (d, *J* = 8.9 Hz, 1H), 3.83 (s, 3H), 3.56 – 3.48 (m, 2H), 2.99 – 2.92 (m, 2H), 2.35 (s, 3H). **^{13}C NMR (120 MHz, Chloroform-*d*) δ** 166.96, 159.92, 156.16, 153.29, 147.94, 147.33, 132.47, 126.01, 121.67, 114.03, 111.05, 56.79, 40.77, 29.75, 22.57. **HRMS:** m/z: For $C_{15}H_{17}N_3O_3$ ([M + H]+): 288.1339, found 288.1332.

6l: 2-hydroxy-4-methoxy-N-(2-(4-methylpyrimidin-5-yl) ethyl) benzamide

^{1}H NMR (500 MHz, DMSO-d_6) δ 11.60 (s, 1H), 8.77 (d, *J* = 1.7 Hz, 1H), 8.35 (d, *J* = 1.6 Hz, 1H), 8.14 (t, *J* = 5.0 Hz, 1H), 7.74 (d, *J* = 8.4 Hz, 1H), 6.69 (dd, *J* = 8.4, 2.3 Hz, 1H), 6.50 (d, *J* = 2.4 Hz, 1H), 3.75 (s, 3H), 3.51 (td, *J* = 6.0, 4.9 Hz, 2H), 2.94 (t, *J* = 6.1 Hz, 2H), 2.32 (s, 3H). **^{13}C NMR (120 MHz, Chloroform-*d*) δ** 169.01, 164.58, 161.76, 159.92, 156.16, 153.29, 132.52, 130.05, 108.64, 103.72, 100.10, 55.34, 39.83, 28.95, 21.34. **HRMS:** m/z: For $C_{15}H_{17}N_3O_3$ ([M + H]+): 288.1335, found 288.1335.

6m: 4-(benzyloxy)-N-(2-(4-methylpyrimidin-5-yl)ethyl)benzamide

^{1}H NMR (500 MHz, DMSO-d_6) δ 8.73 (d, *J* = 1.7 Hz, 1H), 8.63 (t, *J* = 5.1 Hz, 1H), 8.40 (d, *J* = 1.6 Hz, 1H), 7.79 (d, *J* = 8.3 Hz, 2H), 7.45 (dd, *J* = 7.1, 1.4 Hz, 2H), 7.37 (t, *J* = 6.8 Hz, 2H), 7.33 – 7.25 (m, 1H), 7.00 – 6.94 (m, 2H), 5.06 (s, 2H), 3.51 (td, *J* = 6.0, 4.9 Hz, 2H), 2.91 (t, *J* = 6.1 Hz, 2H), 2.31 (s, 3H). **^{13}C NMR (120 MHz, Chloroform-*d*) δ** 167.91, 162.47, 159.92, 156.16, 153.29, 136.17, 132.47, 129.55, 128.39, 127.92 (d, *J* = 14.6 Hz), 127.38, 115.09, 69.54, 39.32, 28.95, 21.63. **HRMS:** m/z: For $C_{21}H_{21}N_3O_2$ ([M + H]+): 348.1754, found 348.1751.

6n: N-(2-(4-methylpyrimidin-5-yl)ethyl)acetamide

^{1}H NMR (500 MHz, DMSO-d_6) δ 8.82 (d, *J* = 1.7 Hz, 1H), 8.33 (d, *J* = 1.6 Hz, 1H), 8.00 (t, *J* = 5.2 Hz, 1H), 3.39 – 3.31 (m, 2H), 2.93 – 2.86 (m, 2H), 2.35 (s, 3H), 1.80 (s, 3H). **^{13}C NMR (120 MHz, Chloroform-*d*) δ** 170.44, 159.92, 156.16, 153.26, 132.23, 39.32, 29.24, 22.86, 21.13. **HRMS:** m/z: For $C_9H_{13}N_3O$ ([M + H]+): 180.1123, found 180.1123.

6o: N-(2-(4-methylpyrimidin-5-yl)ethyl)propionamide

^{1}H NMR (500 MHz, DMSO-d_6) δ 8.69 (d, *J* = 1.7 Hz, 1H), 8.36 (d, *J* = 1.6 Hz, 1H), 7.62 (t, *J* = 4.5 Hz, 1H), 3.38 (td, *J* = 6.2, 4.6 Hz, 2H), 2.91 (t, *J* = 6.2 Hz, 2H), 2.35 (s, 3H), 2.21 (q, *J* = 7.3 Hz, 2H), 1.14 (t, *J* = 7.3 Hz, 3H). **^{13}C NMR (120 MHz, Chloroform-*d*) δ** 173.13, 159.92, 156.16, 153.26, 132.31, 40.32, 39.39, 29.46, 21.34, 10.54. **HRMS:** m/z: For $C_{10}H_{15}N_3O$ ([M + H]+): 194.1306, found 194.1302.

6p: N-(2-(4-methylpyrimidin-5-yl)ethyl)butyramide

^{1}H NMR (500 MHz, DMSO-d_6) δ 8.71 (d, *J* = 1.7 Hz, 1H), 8.40 (d, *J* = 1.6 Hz, 1H), 7.61 (t, *J* = 4.9 Hz, 1H), 3.37 (td, *J* = 6.2, 4.9 Hz, 2H), 2.91 (t, *J* = 6.2 Hz, 2H), 2.35 (s, 3H), 2.16 (t, *J* = 6.5 Hz, 2H), 1.52 (dtd, *J* = 14.0, 7.6, 6.3 Hz, 2H), 0.91 (t, *J* = 7.5 Hz, 3H). **^{13}C NMR (120 MHz, Chloroform-*d*) δ** 172.93, 159.92, 156.16, 153.26, 132.31, 40.27, 38.72, 29.97, 21.82, 19.84, 13.88. **HRMS:** m/z: For $C_{11}H_{17}N_3O$ ([M + H]+): 208.1425, found 208.1425.

6q: 2-hydroxy-N-(2-(4-methylpyrimidin-5-yl) ethyl) acetamide

^{1}H NMR (500 MHz, DMSO-d_6) δ 8.73 (d, *J* = 1.7 Hz, 1H), 8.40 (d, *J* = 1.6 Hz, 1H), 8.21 (t, *J* = 4.6 Hz, 1H), 4.73 (t, *J* = 5.7 Hz, 1H), 4.05 (d, *J* = 5.7 Hz, 2H), 3.31 (td, *J* = 6.2, 4.5 Hz, 2H), 2.85 (t, *J* = 6.2 Hz, 2H), 2.32 (s, 3H). **^{13}C NMR (120 MHz, Chloroform-*d*) δ** 171.89, 159.92, 156.16, 153.26, 132.34, 61.72, 40.77, 30.19, 22.07. **HRMS:** m/z: For $C_9H_{13}N_3O_2$ ([M + H]+): 196.1107, found 196.1105.

6r: 3-((2-(4-methylpyrimidin-5-yl) ethyl) amino)-3-oxopropanoic acid

^{1}H NMR (500 MHz, DMSO-d_6) δ 12.90 (s, 1H), 8.82 (d, *J* = 1.7 Hz, 1H), 8.69 (t, *J* = 4.9 Hz, 1H), 8.40 (d, *J* = 1.6 Hz, 1H), 3.40 (td, *J* = 6.2, 4.8 Hz, 2H), 3.27 (s, 2H), 2.90 (t, *J* = 6.2 Hz, 2H), 2.35 (s, 3H). **^{13}C NMR (120 MHz, Chloroform-*d*) δ** 171.46, 170.66, 159.92, 156.16, 153.26, 132.29, 43.52, 40.55, 30.98, 22.58. **HRMS:** m/z: For $C_{10}H_{13}N_3O_3$ ([M + H]+): 224.1096, found 224.1905.

Molecular Docking

The molecular docking study evaluated the binding affinities of 18 amide-functionalized pyrimidine hybrids (6a–6r) against two critical anticancer targets: epidermal growth factor receptor (EGFR, PDB: 6LUD) and cyclin-dependent kinase 4 (CDK-4, PDB: 7SJ3). The docking scores (in kcal/mol) displayed in **Table 1** provide valuable insights into the potential inhibitory activity of these compounds, where more negative values indicate stronger binding interactions.

Table 1: Docking scores of amide-functionalized pyrimidine hybrids

Compound	R	Target	
		EGFR (6LUD)	CDK-4 (7SJ3)
6a	Phenyl	-5.811	-5.727
6b	2-hydroxy phenyl	-6.957	-8.45
6c	3-nitro phenyl	-5.098	-6.225
6d	3-bromo phenyl	-6.704	-6.061
6e	3-chloro phenyl	-6.544	-5.998
6f	4-methyl phenyl	-5.492	-7.959
6g	4-methoxy phenyl	-6.059	-5.96
6h	2,4-dichloro phenyl	-6.112	-6.621
6i	3,5-dinitro phenyl	-5.368	-5.82
6j	3,4-dihydroxy phenyl	-7.215	-8.72
6k	4-hydroxy,3-methoxy phenyl	-7.245	-6.919
6l	2-hydroxy,4-methoxy phenyl	-6.884	-9.23
6m	4-benzyloxy phenyl	-4.993	-6.675
6n	Methyl	-5.763	-6.352
6o	Ethyl	-5.839	-6.635
6p	Propyl	-5.961	-6.745
6q	Hydroxy methyl	-6.623	-6.016
6r	Malonyl	-6.03	-7.896

EGFR (6LUD) Binding Affinity

The docking scores for EGFR ranged from -4.993 (6m) to -7.245 (6k), demonstrating moderate to strong binding for most compounds. The highest-affinity ligands were 6k (4-hydroxy-3-methoxyphenyl, -7.245) (Figure 3), 6j (3,4-dihydroxyphenyl, -7.215) (Figure 3), and 6b (2-hydroxyphenyl, -6.957) (Figure 3), suggesting that polar substituents, particularly hydroxyl groups, significantly enhance binding. The presence of hydroxy and methoxy groups likely facilitates hydrogen bonding with key residues in the EGFR active site. Conversely, bulky substituents such as the 4-benzyloxy group in 6m (-4.993) and electron-withdrawing nitro groups (6c, 3-nitrophenyl, -5.098) weakened binding, possibly due to steric clashes or unfavourable electrostatic interactions.

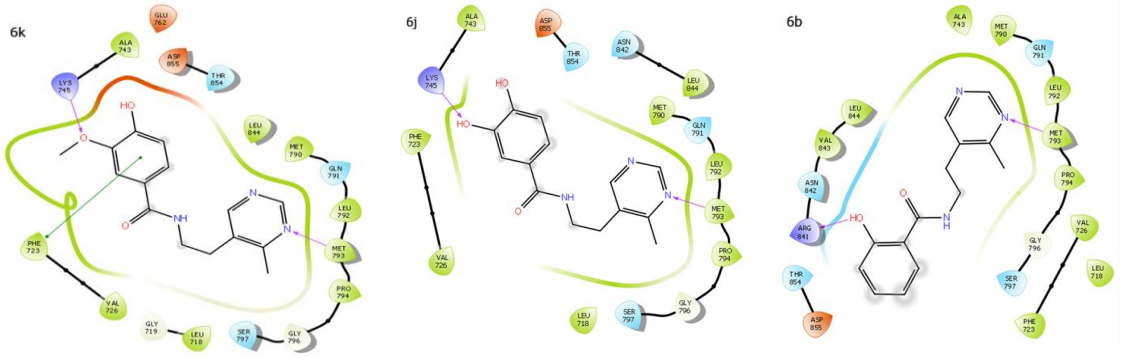

Figure 3: Interactions of Compounds 6k, 6j and 6b at the active site of EGFR (6LUD) protein

CDK-4 (7SJ3) Binding Affinity

The CDK-4 docking scores exhibited a broader range, from -5.727 (6a) to -9.23 (6l), indicating that several compounds exhibit high-affinity binding. The most potent inhibitor was 6l (2-hydroxy-4-methoxyphenyl, -9.23) (Figure 4), followed by 6j (3,4-dihydroxyphenyl, -8.72) (Figure 4) and 6b (2-hydroxyphenyl, -8.45) (Figure 4), reinforcing the importance of hydrogen-bonding interactions. Notably, 6f (4-methylphenyl, -7.959) and 6r (malonyl, -7.896) also displayed strong binding, suggesting that both hydrophobic and polar interactions contribute to CDK-4 inhibition. In contrast, unsubstituted phenyl (6a, -5.727) and chloro-substituted derivatives (6e, -5.998) showed weaker binding, highlighting the necessity of optimized substituents for effective inhibition.

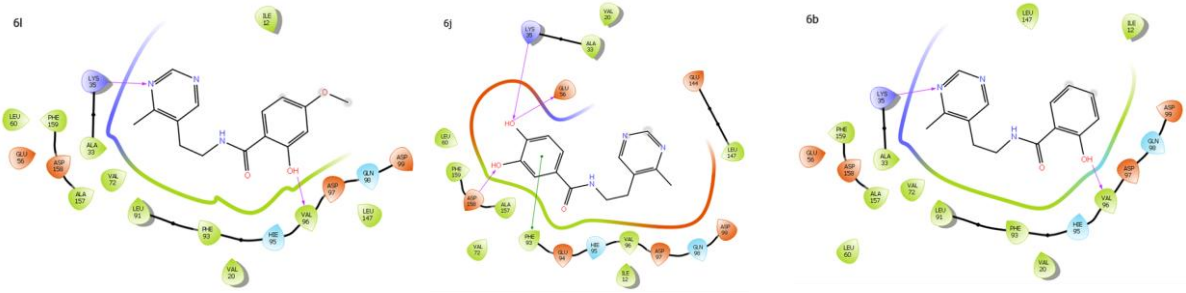

Figure 4: Interactions of Compounds 6l, 6j and 6b at the active site of CDK-4 (7SJ3) protein

A comparative analysis revealed that certain compounds exhibit dual-targeting potential, particularly 6j, 6l, and 6b, which showed high affinity for both EGFR and CDK-4. However, some derivatives displayed target selectivity: 6k (4-hydroxy-3-methoxyphenyl) was more potent against EGFR (-7.245) than CDK-4 (-6.919), while 6f (4-methylphenyl) was more selective for CDK-4 (-7.959 vs. -5.492 for EGFR). This differential binding suggests that minor structural modifications can fine-tune selectivity, which may be exploited in drug design to minimize off-target effects.

The docking results highlight several important structures activity relationships for the amide-functionalized pyrimidine hybrids. Hydroxyl substitutions, such as the 2-hydroxy group in compound 6b and the 3,4-dihydroxy configuration in 6j, markedly improved binding affinity toward both EGFR and CDK-4 targets. This enhancement is likely attributed to their ability to form stabilizing hydrogen bonds with key catalytic residues within the binding pockets. In contrast, the introduction of bulky or strongly electron-withdrawing groups, such as nitro (NO_2) or benzyloxy moieties, resulted in a noticeable reduction in binding affinity. This may stem from steric hindrance within the active site or disruption of favorable electrostatic interactions. Furthermore, derivatives featuring dual substitutions, particularly hydroxy-methoxy combinations as seen in compound 6l, consistently outperformed their monosubstituted counterparts, suggesting potential synergistic interactions that enhance target engagement. Lastly, the alkyl-substituted derivatives (6n–6q) demonstrated moderate binding activity, with the propyl-substituted compound 6p showing the most favorable interaction. This observation implies that the length and flexibility of the alkyl chain play a role in modulating the binding conformation and interactions within the receptor site.

Table 2: IC50 values of amide-functionalized pyrimidine hybrids (6a-6r)

Compound	R	Non-Small Cell Lung Cancer line (A-549) Avg±SD	Colorectal Cancer cell line (HCT-116) Avg±SD	Pancreatic cancer cell line (PANC-1) Avg±SD	Cervical cancer cell line (HaLa) Avg±SD	Human Embryonic Kidney Cell line (HEK-293) Avg±SD
6a	Phenyl	14.91 ± 2.08	16.00 ± 1.26	19.15 ± 0.89	14.43 ± 1.79	36.09 ± 2.79
6b	2-hydroxy phenyl	6.95 ± 1.05	10.65 ± 1.04	9.72 ± 2.07	5.38 ± 1.04	38.21 ± 2.12
6c	3-nitro phenyl	14.20 ± 2.11	18.21 ± 1.29	19.37 ± 0.91	15.74 ± 1.83	36.82 ± 2.84
6d	3-bromo phenyl	13.05 ± 1.08	12.83 ± 1.06	13.86 ± 2.10	15.38 ± 1.06	35.06 ± 2.17
6e	3-chloro phenyl	14.61 ± 1.78	18.38 ± 1.77	19.30 ± 1.06	21.32 ± 4.05	30.27 ± 1.84
6f	4-methyl phenyl	15.75 ± 1.85	20.66 ± 1.18	16.25 ± 1.06	23.66 ± 2.71	29.65 ± 3.30
6g	4-methoxy phenyl	13.91 ± 3.15	18.76 ± 1.72	19.59 ± 2.06	19.84 ± 2.62	38.52 ± 1.43
6h	2,4-dichloro phenyl	17.87 ± 1.24	16.70 ± 1.28	19.11 ± 1.11	17.53 ± 2.05	38.00 ± 1.23
6i	3,5-dinitro phenyl	23.28 ± 4.06	25.13 ± 2.24	16.21 ± 3.37	26.93 ± 3.63	41.63 ± 1.70
6j	3,4-dihydroxy phenyl	8.97 ± 1.74	5.67 ± 1.74	7.52 ± 1.03	9.47 ± 3.97	33.64 ± 4.79
6k	4-hydroxy,3-methoxy phenyl	8.96 ± 1.30	10.97 ± 1.46	12.68 ± 2.06	9.82 ± 1.20	41.98 ± 0.98
6l	2-hydroxy,4-methoxy phenyl	5.87 ± 3.13	8.18 ± 1.18	6.82 ± 3.92	7.86 ± 1.69	34.27 ± 1.48
6m	4-benzyloxy phenyl	22.31 ± 2.76	18.84 ± 3.19	23.74 ± 1.49	19.21 ± 3.52	38.74 ± 1.74
6n	Methyl	20.40 ± 1.99	18.38 ± 1.17	20.83 ± 1.05	18.32 ± 2.71	35.48 ± 1.36
6o	Ethyl	21.05 ± 2.26	16.04 ± 3.19	23.93 ± 2.58	19.55 ± 3.63	37.32 ± 1.70
6p	Propyl	18.89 ± 1.26	20.10 ± 2.10	19.56 ± 1.16	18.40 ± 1.13	35.71 ± 2.64
6q	Hydroxy methyl	18.65 ± 3.15	20.52 ± 1.46	27.13 ± 2.05	27.20 ± 2.61	41.97 ± 1.14
6r	Malonyl	12.42 ± 1.27	14.43 ± 1.44	13.22 ± 2.01	14.08 ± 1.18	41.10 ± 0.96
Doxorubicin		1.49±0.52	1.78±0.61	1.95±0.32	1.88±0.57	3.56±0.65

Anticancer activity

Comparative Analysis of Cytotoxic Potency

Non-Small Cell Lung Cancer (A-549)

The A-549 cell line exhibited the most robust response to hydroxy-substituted derivatives, with compound 6l (2-hydroxy-4-methoxyphenyl) emerging as the most potent inhibitor (IC50 = 5.87 µM). This was closely followed by 6b (2-hydroxyphenyl, 6.95 µM) and the dihydroxy/methoxy analogs 6j and 6k (8.97 and 8.96 µM, respectively). The superior activity of these compounds suggests that hydrogen bond donor-acceptor capabilities are crucial for interaction with molecular targets in lung cancer cells. In contrast, compounds bearing electron-withdrawing nitro groups (6c, 14.20 µM) or bulky substituents (6m, 22.31 µM) showed significantly reduced potency, likely due to impaired target engagement or cellular uptake.

Colorectal Cancer (HCT-116)

The HCT-116 results revealed an exceptional sensitivity to compound 6j (3,4-dihydroxyphenyl,

5.67 µM), which was nearly twice as potent as its closest analog 6l (8.18 µM). This remarkable activity suggests that the meta-para dihydroxy configuration may be particularly favorable for targeting colorectal cancer pathways. The consistent performance of hydroxy-substituted compounds contrasted sharply with the weak activity of methyl (6f, 20.66 µM) and nitro (6i, 25.13 µM) derivatives, reinforcing the importance of polar functional groups for anticancer activity in this cell line.

Pancreatic Cancer (PANC-1)

The PANC-1 results mirrored the trends observed in other cell lines, with compounds 6l (6.82 µM), 6j (7.52 µM), and 6b (9.72 µM) demonstrating the strongest inhibition. The approximately 3-4 fold difference in potency between these lead compounds and the least active derivative 6q (27.13 µM) highlights the critical nature of substituent selection. Notably, the hydroxymethyl derivative 6q showed particularly poor activity across all cancer types, suggesting this modification may interfere with target binding or cellular penetration.

Cervical Cancer (HaLa)

The HaLa cell line displayed the greatest sensitivity to compound 6b (5.38 µM), followed by 6l (7.86 µM) and 6j (9.47 µM). This pattern confirms the consistent superiority of hydroxy-substituted analogs across diverse cancer types. The dramatic difference between 6b and the least active compounds (6i and 6q, both >26 µM) represents a nearly 5-fold potency range, providing clear evidence for structure-dependent activity.

The HEK-293 normal cell line results revealed that all test compounds exhibited significantly higher IC50 values (29.65-41.98 µM) compared to their cancer cell line activities, indicating favorable selectivity profiles. Particularly noteworthy were compounds 6b, 6j, and 6l, which maintained 3-7-fold selectivity for cancer cells over normal cells. This selectivity window compares favorably with doxorubicin, which showed only minimal separation between its cytotoxic effects on cancer (1.49-1.95 µM) and normal cells (3.56 µM). The higher IC50 values in HEK-293 cells suggest that the pyrimidine hybrids may exploit cancer-specific vulnerabilities while sparing normal cells, a crucial advantage for potential therapeutic applications.

Structure-Activity Relationship Analysis

The consistent top performance of hydroxy-substituted derivatives across all cancer cell lines provides compelling evidence for the critical role of these functional groups. The ortho-hydroxy substitution in 6b appears particularly favorable, likely due to optimal spatial positioning for hydrogen bonding with target proteins. The enhanced activity of 6j (3,4-dihydroxyphenyl) suggests that additional hydrogen bond donor capacity can further improve potency, especially in colorectal cancer. The exceptional performance of 6l (2-hydroxy-4-methoxyphenyl) indicates that combining hydrogen bonding (OH) with moderate lipophilicity (OCH3) creates an optimal balance for cellular penetration and target interaction.

Electron-withdrawing groups generally diminished activity, with nitro-substituted compounds (6c, 6i) consistently ranking among the least potent derivatives. This suggests that maintaining electron density on the aromatic ring may be important for target binding. The notable exception was 6d (3-bromophenyl), which showed intermediate activity, possibly due to halogen bonding potential. The poor performance of dinitro derivative 6i (IC50 >23 µM across all cell lines) provides particularly strong evidence against using strong electron-withdrawing groups in this series.

Bulky substituents such as the benzyloxy group in 6m consistently reduced potency, likely due to steric interference with target binding or membrane penetration. This trend was most apparent in the pancreatic cancer cell line, where 6m (23.74 µM) was nearly 4-fold less active than 6l (6.82 µM). The moderate activity of halogenated compounds (6d, 6e, 6h) suggests that smaller hydrophobic groups may be tolerated but do not enhance activity compared to hydroxy/methoxy substitutions.

The consistent pattern of activity across diverse cancer cell lines suggests that the most potent compounds may act through common molecular targets rather than cell type-specific mechanisms. The strong correlation between MTT assay results and previously reported EGFR/CDK-4 docking scores supports kinase inhibition as a likely primary mechanism. The superior activity of hydroxy-substituted derivatives aligns perfectly with their predicted ability to form hydrogen bonds in kinase ATP-binding pockets. The differential activity between cancer and normal cells may reflect either increased dependence on targeted kinases in malignant cells or enhanced accumulation in tumor tissue due to altered metabolism.

This comprehensive analysis of amide-functionalized pyrimidine hybrids has identified several compounds with significant anticancer potential. The clear structure-activity relationships established through this study provide a robust foundation for rational drug design, with hydroxy and methoxy substitutions emerging as critical determinants of potency. The exceptional performance of compounds 6b, 6j, and 6l, coupled with their favorable selectivity profiles,

positions them as strong candidates for further development as potential anticancer therapeutics.

Correlation of molecular docking results and anticancer activity

The molecular docking studies and anticancer activity results demonstrate a strong correlation between the predicted binding affinities of the amide-functionalized pyrimidine hybrids and their observed cytotoxic effects, supporting kinase inhibition as the primary mechanism of action. The most active compounds in both experimental systems - particularly 6b (2-hydroxyphenyl), 6j (3,4-dihydroxyphenyl), and 6l (2-hydroxy-4-methoxyphenyl) - consistently showed superior performance, with these hydroxy-substituted derivatives exhibiting the strongest binding to both EGFR and CDK-4 targets in silico and the most potent anticancer activity in cellular assays. The exceptional docking scores for 6l (-7.245 kcal/mol for EGFR and -9.23 kcal/mol for CDK-4) directly paralleled its outstanding cytotoxicity across all cancer cell lines (IC50 values of 5.87-7.86 µM), suggesting its broad-spectrum activity results from effective dual kinase inhibition. Similarly, 6j's remarkable potency against HCT-116 cells (IC50 = 5.67 µM) aligns with its predicted strong binding to CDK-4 (-8.72 kcal/mol), indicating this dihydroxy configuration may preferentially target colorectal cancer pathways.

The structure-activity relationships observed in both systems consistently highlighted the critical importance of hydroxy groups for biological activity, with these polar substituents enabling optimal hydrogen bonding interactions in the kinase binding pockets while also enhancing cellular potency. The synergistic effect of combining hydroxy and methoxy groups, as seen in compound 6l, was particularly noteworthy - this modification appeared to balance target engagement (through hydrogen bonding) with improved membrane permeability (through moderate lipophilicity). Conversely, compounds featuring electron-withdrawing nitro groups or bulky substituents uniformly showed weaker binding in docking studies and reduced cytotoxicity, confirming that steric hindrance and unfavorable electronic effects impair both target interaction and cellular activity. The parallel trends extended to selectivity profiles as well, with the most promising compounds (6b, 6j, 6l) maintaining 3-7-fold greater potency against cancer cells versus normal HEK-293 cells, consistent with the known overexpression of EGFR and CDK-4 in malignant cells.

The exceptional performance of lead compounds 6b, 6j and 6l across both evaluation platforms positions them as particularly promising candidates for continued development as targeted therapeutics against multiple cancer types.

CONCLUSION

In this study, a series of amide-functionalized pyrimidine hybrids (6a–6r) were synthesized via a concise three-step route and evaluated for their anticancer potential through molecular docking and in vitro cytotoxicity assays. The synthetic pathway offered good yields and structural versatility, enabling systematic structure–activity relationship (SAR) analysis. Molecular docking against EGFR and CDK-4 revealed that hydroxy-substituted derivatives, particularly 6b (2-hydroxyphenyl), 6j (3,4-dihydroxyphenyl), and 6l (2-hydroxy-4-methoxyphenyl), exhibited the most favorable binding energies, suggesting strong potential for dual kinase inhibition. These findings were corroborated by cytotoxicity data across four human cancer cell lines (A-549, HCT-116, PANC-1, and HeLa), where the same compounds consistently demonstrated potent activity with IC_{50} values ranging from 5.38 to 9.72 µM and maintained favorable selectivity over normal HEK-293 cells. SAR analysis underscored the importance of hydrogen-bonding functionalities for target engagement and anticancer efficacy, while bulky or strongly electron-withdrawing substituents impaired both binding affinity and cellular potency. The strong correlation between in silico docking results and in vitro cytotoxicity supports kinase inhibition, particularly of EGFR and CDK-4, as the likely mechanism of action. Overall, the lead compounds 6b, 6j, and 6l emerge as promising scaffolds for further development as selective, multi-targeted anticancer agents.

COMPETING INTERESTS

The authors have declared that no competing interest exists.

REFERENCES

1. Siegel, R.L., Miller, K.D., Wagle, N.S. & Jemal, A. (2023). Cancer statistics, 2023. CA Cancer J Clin., 73(1):17-48. doi: 10.3322/caac.21763.
2. Alafeefy, A.M., Ceruso, M., Al-Tamimi, A.M., Del Prete, S., Capasso, C. & Supuran, C.T. (2014). Quinazoline-sulfonamides with potent inhibitory activity against the α-carbonic anhydrase from Vibrio cholerae. Bioorg Med Chem., 22(19):5133-5140. doi: 10.1016/j.bmc.2014.08.015.
3. Alafeefy, A.M., Ceruso, M., Al-Jaber, N.A., Parkkila, S., Vermelho, A.B. & Supuran, C.T. (2015). A new class of quinazoline-sulfonamides acting as efficient inhibitors against the α-carbonic anhydrase from Trypanosoma cruzi. J Enzyme Inhib Med Chem., 30(4):581-585. doi: 10.3109/14756366.2014.956309.

4. DeMartino, J.K. & Boger, D.L. (2008). Glycinamide ribonucleotide transformylase (GAR Tfase) as a target for cancer therapy. Drugs Fut., 33(11):969. doi: 10.1358/dof.2008.33.11.1247542.
5. Curran, W.J. (2002). New chemotherapeutic agents: update of major chemoradiation trials in solid tumors. Oncology (Williston Park), 63 Suppl 2:29-38. doi: 10.1159/000067145.
6. Nurgali, K., Jagoe, R.T. & Abalo, R. (Eds.). (2018). Adverse effects of cancer chemotherapy: Anything new to improve tolerance and reduce sequelae? Front Pharmacol., 9:245. doi: 10.3389/fphar.2018.00245.
7. El-Messery, S.M., Hassan, G.S., Nagi, M.N., Habib, E.E., Al-Rashood, S.T. & El-Subbagh, H.I. (2016). Synthesis, biological evaluation and molecular modeling study of some new methoxylated 2-benzylthio-quinazoline-4(3H)-ones as nonclassical antifolates. Bioorg Med Chem Lett., 26(19):4815-4823. doi: 10.1016/j.bmcl.2016.08.022.
8. Arteaga, C.L. & Johnson, D.H. (2001). Tyrosine kinase inhibitors—ZD 1839 (Iressa). Curr Opin Oncol., 13(6):491-498. doi: 10.1097/00001622-200111000-00012.
9. Barker, A.J., Gibson, K.H., Grundy, W., Godfrey, A.A., Barlow, J.J., Healy, M.P., et al. (2001). Studies leading to the identification of ZD 1839 (iressa™): an orally active, selective epidermal growth factor receptor tyrosine kinase inhibitor targeted to the treatment of cancer. Bioorg Med Chem Lett., 11(14):1911-1914. doi: 10.1016/s0960-894x(01)00344-4.
10. Barker, J. & Johnstone, C. (1997). Preparation of 4-anilino-7-heteroarylquinazolines as tyrosine kinase inhibitors. World Intellectual Property Organization Patent., WO97/30044 A1.
11. El-Azab, A.S., Al-Omar, M.A., Abdel-Aziz, A.A., Abdel-Aziz, N.I., El-Sayed, M.A., Aleisa, A.M., et al. (2010). Design, synthesis and biological evaluation of novel quinazoline derivatives as potential antitumor agents: molecular docking study. Eur J Med Chem., 45(9):4188-4198. doi: 10.1016/j.ejmech.2010.06.013.
12. Tiwari, S., Sachan, S., Mishra, A., Tiwari, S. & Pandey, V. (2015). The anticancer activity of some novel 4-anilino quinazoline derivatives as tyrosine kinase (EGFR) inhibitor and the quantitative structure activity relationships. Int J Pharm Life Sci., 6(12):4819-4828.
13. Al-Suwaidan, I.A., Abdel-Aziz, A.A., Shawer, T.Z., Ayyad, R.R., Alanazi, A.M., El-Morsy, A.M., et al. (2016). Synthesis, antitumor activity and molecular docking study of some novel 3-benzyl-4(3H) quinazolinone analogues. J Enzyme Inhib Med Chem., 31(1):78-89. doi: 10.3109/14756366.2015.1004059.
14. Ammazzalorso, A., Agamennone, M., De Filippis, B. & Fantacuzzi, M. (2021). Development of CDK4/6 Inhibitors: A Five Years Update. Molecules., 26(5):1488. doi: 10.3390/molecules26051488.
15. Suzuki, H., Sakai, N., Iwahara, R., Fujiwaka, T., Satoh, M. & Kakehi, A. (2007). Novel synthesis of 7-fluoro-8-(trifluoromethyl)-1H-1,6-naphthyridin-4-one derivatives: Intermolecular cyclization of an N-Silyl-1-azaallyl anion with Perfluoroalkene and subsequent intramolecular skeletal transformation of the resulting pentasubstituted pyridines. J Org Chem., 72(15):5878-5881. doi: 10.1021/jo070564m.
16. Sakai, N., Aoki, D., Hamajima, T. & Konakahara, T. (2006). Yb (OTf)3-catalyzed cyclization of an N-silylen amine with 2- methylene-1, 3-cyclohexanedione to afford a 7,8-dihydroquinolin-5(6H)-one derivative and its application to the one-pot conversion to a 2, 3, 5-trisubstituted quinoline derivative. Tetrahedron Lett., 47(8):1261-1265. doi: 10.1016/j.tetlet.2005.12.080.
17. Konakahara, T., Sakai, N., Hattori, N., Tomizawa, N. & Abe, N. (2005). New approach to the synthesis of non-benzenoid aromatic compounds, functionalized 1-Azaazulene derivatives: Cyclization reactions of 2-substituted tropones with N-Silylenamine and enamine. Heterocycles., 65(11):2799. doi: 10.3987/COM-05-10537.
18. Stanovnik, B. and Svete, J. (2004). Synthesis of heterocycles from alkyl 3- (dimethyl amino) propenoates and related enaminones. Chem Rev., 104(5):2433-2480. doi: 10.1021/cr020093y.
19. House, H.O. (1972). Modern Synthetic Reactions. 2nd ed. Menlo Park: Benjamin / Cummings.
20. Larock, R.C. (1999). Comprehensive Organic Transformations. 2nd ed. New York: Wiley-VCH.
21. Ghosh, A.K. & Shahabi, D. (2021). Synthesis of amide derivatives for electron deficient amines and functionalized carboxylic acids using EDC and DMAP and a catalytic amount of HOBt as the coupling reagents. Tetrahedron Lett., 63:152719. doi: 10.1016/j.tetlet.2020.152719.
22. Meng, X.Y., Zhang, H.X., Mezei, M. & Cui, M. (2011). Current Computer Aided-Drug Design. Curr Comput Aided Drug Des., 7(2):146-157.
23. Riss, T.L., Moravec, R.A., Niles, A.L., Duellman, S., Benink, H.A. & Worzella, T.J. (2016). Cell Viability Assays. In: Assay Guidance Manual [Internet]. Bethesda (MD): National Center for Advancing Translational Sciences. https://www.ncbi.nlm.nih.gov/books/NBK144065/.